View Article Online / Journal Homepage / Table of Contents for this issue
Dynamic Article Links

CrystEngComm

Cite this: *CrystEngComm*, 2012, **14**, 1990

www.rsc.org/crystengcomm

PAPER

Simple chemical preparation of perovskite-based materials using alkali treatment†

Po-Chin Chen,[a] Min-Chiao Tsai,[a] Yi-Jen Huang,[a] Hsin-Tien Chiu[b] and Chi-Young Lee*[a]

Received 28th November 2011, Accepted 10th January 2012
DOI: 10.1039/c2ce06598c

In this work, a simple alkali treatment process was introduced to synthesize ABO_3 perovskite related materials: $CaTiO_3$ (CTO), $SrTiO_3$ (STO), $BaTiO_3$ (BTO) and $Ba_xSr_{1-x}TiO_3$ (BST). The perovskite materials, synthesized by using stoichiometric amounts of corresponding alkaline solutions $Ba(OH)_2$, $Sr(OH)_2$, $Ca(OH)_2$ and powdered TiO_2, are pure phase and well-crystallized. The obtained powders are round, round-edged cubes and cubes with sharp edges for $BaTiO_3$, $SrTiO_3$ and $CaTiO_3$ respectively. What's more, the Ba content (x) in BST can be directly and precisely modified to be any value between one and zero. And, the morphology of $SrTiO_3$ can be manipulated by altering the reaction time. As time is prolonged, the morphology of the product changes from round to round-edged cubes to sharp-edged cubes. In the future, materials with such specific microstructure and morphologies may be used in electro-optical and photocatalytic applications.

Published on 30 January 2012. Downloaded by National Chiao Tung University on 28/04/2014 23:26:24.

Introduction

Perovskite-based compounds possess ferroelectric and anti-ferroelectric properties and are widely used in electro-optical and electromechanical devices. Some with high dielectric constants are used to produce capacitors in the semiconductor industry. Many synthetic methods of ABO_3 have been reported over the last decade, such as solid-state reactions,[1] CVD method[2] and sol–gel method.[3] The conventional preparation of these electro-ceramics by solid-state reactions employs metal oxides, for example AO and BO_2 for synthesis of ABO_3. However, this process requires multiple cycles of milling and calcinations at high temperatures to achieve complete mixing and crystallization.[1] Also, the powders are agglomerated grains of diverse sizes and often contaminated with abrasive particles or unreacted materials. Furthermore, the fabrication of $(A_xA_{1-x}'BO_3)$ perovskites is hard to manipulate because the starting materials are non-homogeneous mixtures and unexpected precipitation of ABO_3 or $A'BO_3$ occurs during calcinations. In contrast, the sol–gel process uses organometallic compounds as precursors, providing a molecular-level mixing of the individual components to yield submicrometre crystalline materials at low temperatures without calcination.[3] However, in order to get $(A_xA_{1-x}'BO_3)$ perovskites, many organometallic precursors need to be introduced to the reaction mixture. The different reaction rates of organometallic compounds result in variation of the composition and to prevent this, extra precursors or chelating agents would be added during synthesis.[4] Still, this causes impurities and structural defects. Moreover, cost, moisture sensitivity of the precursors and precise reaction conditions are fatal disadvantages for the sol–gel process to be scaled up.

Until today, reports on low-temperature synthesis of well-crystallized perovskite materials are sparse and most of them use the sol–gel process.[5,6] Brutchey and Morse reported the lowest temperature to synthesize $BaTiO_3$ at 160 °C by hydrolyzing the bimetallic alkoxide $BaTi[OCH_2CH(CH_3)OCH_3]_6$.[7] However, to the best of our knowledge there are no reports on the synthesis of $(A_xA_{1-x}'BO_3)$ perovskites below 150 °C.

Here we report a simple alkali treatment for synthesis of ABO_3 perovskite related materials with tunable composition and morphology at 140 °C. The formation mechanism and morphology variation were investigated in detail.

Experimental

The following reagents were purchased from the indicated suppliers and used directly: pure anatase phase TiO_2 (Alfa, 99.7%), sodium hydroxide (RDH, 99%), and Group 2 hydroxides: $Ba(OH)_2 \cdot 8H_2O$ (RDH, 98%), $Sr(OH)_2 \cdot 8H_2O$ (Aldrich, 95%) and $Ca(OH)_2$ (RDH, 96%). Distilled water was deionized using a Millipore (Barnstead) system.

$BaTiO_3$ (BTO), $SrTiO_3$ (STO), $CaTiO_3$ (CTO) and $Ba_xSr_{1-x}TiO_3$ (BST) were synthesized by alkali treatment. A typical synthesis procedure of these materials is as follows. 0.01 mol TiO_2 and 0.01 mol corresponding Group 2 hydroxides are mixed

[a]*Department of Materials Science and Engineering, National Tsing Hua University, Hsinchu, 30043, Taiwan, R.O.C. E-mail: cylee@mx.nthu.edu.tw*
[b]*Department of Applied Chemistry, National Chiao Tung University, Hsinchu, 30050, Taiwan, R.O.C.*

† Electronic supplementary information (ESI) available: Fig. S1 SEM image of TiO_2 precursor. Fig. S2 TEM images of (a) $BaTiO_3$ and (b) $SrTiO_3$ small nuclei agglomerate on the surface of TiO_2. See DOI: 10.1039/c2ce06598c

This journal is © The Royal Society of Chemistry 2012

View Article Online

Published on 30 January 2012. Downloaded by National Chiao Tung University on 28/04/2014 23:26:24.

in 100 mL NaOH solution and then refluxed at 140 °C for 48–56 h. The concentration of the whole base solution is 5 M controlled by adding proper NaOH. The amount of NaOH depends on the solubility of the Group 2 hydroxide (*e.g.* 16 g NaOH for the synthesized BTO, STO and BST; 19.98 g NaOH for the synthesized CTO). After refluxing at 140 °C under N_2 atmosphere, the turbid product was separated and collected by centrifugation, washed with DI-water several times to remove the unreacted metal hydroxides and finally dried at 80 °C.

The morphologies and the compositions of the powders were examined using a JEOL 6500 field emission scanning electron microscope (FESEM) equipped with an energy dispersive X-ray spectrometry system (EDS). Moreover, microstructures, crystallinity and morphology details of the powders were investigated using a JEOL 200 CX transmission electron microscope (TEM). The powders were mixed with polymers and then sliced into 70 nm thick samples with a Leica EM UC6 ultramicrotome for TEM observation. The microstructures of the powders were studied using a Bruker D8-advanced diffractometer (XRD) with CuKα radiation.

Results and discussions

BTO, STO, and CTO were successfully synthesized by alkali treatment of TiO_2. Fig. 1 shows the X-ray diffraction patterns of the powders obtained by the reaction of TiO_2 with either $Ba(OH)_2$, $Sr(OH)_2$ or $Ca(OH)_2$ in a 5 M base solution for 2 days. The un-reacted TiO_2 and other impurities are not observed. In Fig. 1, the peaks can be assigned to the cubic $Pm\bar{3}m$ symmetry with $a = b = c = 0.391$ nm for STO and orthorhombic $Pbnm$ symmetry with $a = 5.388$, $b = 5.447$, and $c = 7.654$ nm for CTO, respectively. In Fig. 1(a) and (b), XRD and Raman spectra demonstrate that the synthesized BTO is tetragonal with $P4mm$ symmetry while the values of lattice constants a and c are very close, about 0.400 nm. The above results are consistent with the phase of these perovskite materials at room temperature.

BST of different Ba/Sr ratios can also be obtained by this method. BSTs with $x = 0$, 0.25, 0.5, 0.75, 1 were synthesized by a reaction of stoichiometric amounts of $Ba(OH)_2$ and $Sr(OH)_2$ with TiO_2. Based on the EDS analysis of the products, the Ba, Sr, and Ti contents are consistent with the starting materials used. The XRD peaks contributed by the diffraction of (200) planes of BSTs with various Ba contents are shown in Fig. 2(a). The linear relationship between the lattice constants of BST, estimated by the Bragg equation using the diffraction of the (200) plane, and various Ba contents is shown in Fig. 2(b). Thin and symmetrical peaks imply that there is only a single phase of BST, without the presence of BTO and STO. From the literature, it is difficult to adjust the ratio of the elements in the BST accurately whether the traditional solid state method or the sol–gel process is used.

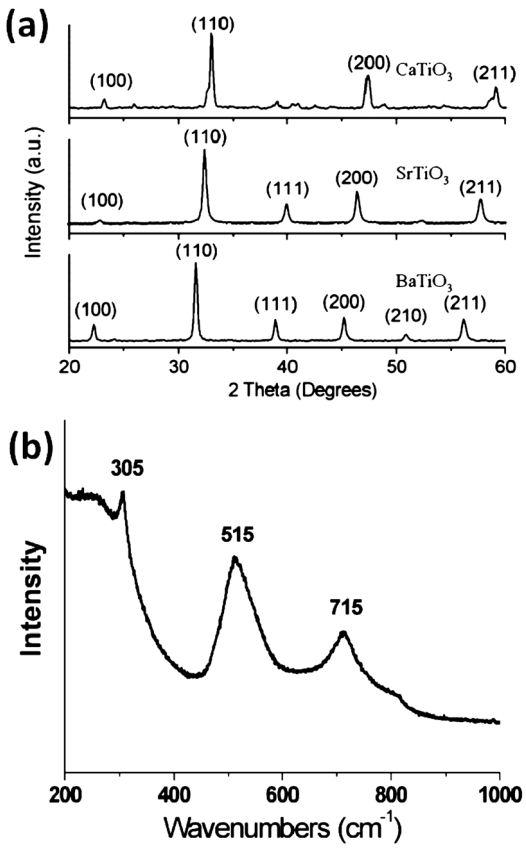

Fig. 1 (a) X-Ray diffraction patterns of synthesized perovskite materials ($BaTiO_3$, $SrTiO_3$, $CaTiO_3$) obtained by the reaction of TiO_2 with the corresponding Group 2 hydroxide in a 5 M base solution for 2 days. (b) Raman spectrum of synthesized $BaTiO_3$.

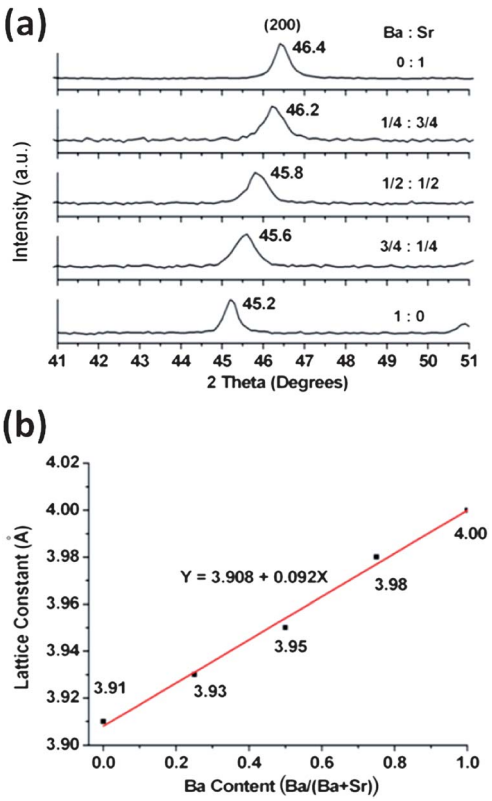

Fig. 2 (a) X-Ray diffraction patterns of synthesized $Ba_xSr_{(1-x)}TiO_3$, where $x = 0$, 0.25, 0.50, 0.75, 1 obtained by the reaction of TiO_2 with stoichiometric amounts of barium and strontium hydroxides in a 5 M base solution for 2 days. (b) The relationship between the lattice constants of BST, estimated by the Bragg equation using the diffraction of the (200) plane, and the various Ba contents.

View Article Online

Published on 30 January 2012. Downloaded by National Chiao Tung University on 28/04/2014 23:26:24.

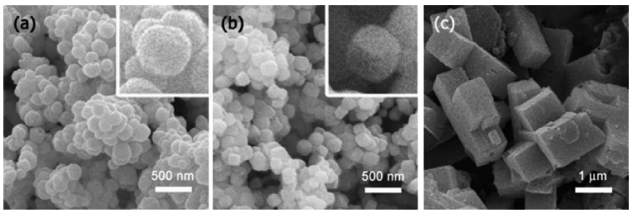

Fig. 3 SEM images of synthesized perovskite materials obtained by the reaction of TiO_2 with the corresponding Group 2 hydroxide in a 5 M base solution for 2 days. (a) $BaTiO_3$ round particles; (b) $SrTiO_3$ round-edged cubes; (c) large cubic $CaTiO_3$ particles with sharp edges.

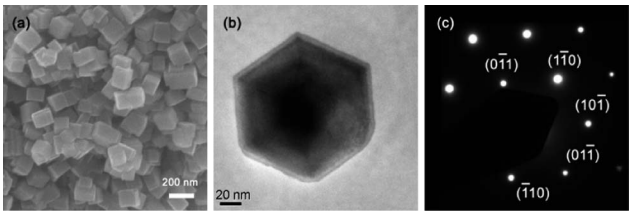

Fig. 5 (a) The SEM image of the synthesized STO obtained by the reaction of TiO_2 with $Sr(OH)_2$ in a 5 M alkaline solution for 56 hours. (b) The TEM image of an individual particle along the diagonal of a cube. (c) The corresponding SAED of the individual particle shown in (b).

However, it can be altered easily by the stoichiometry of the starting materials in this method.[8]

Fig. 3 shows the SEM images of the powders obtained by the reaction of TiO_2 with either $Ba(OH)_2$, $Sr(OH)_2$, or $Ca(OH)_2$ in a 5 M base solution for 2 days. It can be seen in Fig. 3(a) that the synthesized BTO powder consists of spherical particles with diameters of 100–200 nm. Unlike the BTO powder, the synthesized CTO powder consists of cubes with sharp edges and submicrometre sizes as shown in Fig. 3(c). The appearance of the synthesized STO powder can be described as cubes with rounded edges and a side-length of about 150 nm.

The morphology of materials is affected strongly by the stacking rate on different surfaces in a crystal, and the stability of the surfaces.[9–11] Forms of a crystal are both determined by structural factors and the energy of equilibrium states. Firstly, considering the growth rate anisotropy in a cubic structure, if the stacking rates of all surfaces were nearly the same, spherical particles with all surfaces equally exposed were obtained. On the other hand, if the stacking rate on the {100} surfaces is much slower than that of other surfaces, the results are sharp edged cubes with only the {100} facets exposed. Another reason leading to the formation of sharp edged cubes with only {100} facets exposed is the stability of the {100} surfaces. Similar mechanisms have been reported in the literature.[12–14]

In order to learn more about anisotropic growth, the calculations of the cubic structure forms *vs.* stacking rates along ⟨111⟩, ⟨110⟩ and ⟨100⟩ ($R\langle 111\rangle$, $R\langle 110\rangle$ and $R\langle 100\rangle$) directions were executed by using WinXMorph.[17] We found that a sharp edged cube was obtained as $R\langle 111\rangle/R\langle 110\rangle/R\langle 100\rangle \approx >1.8/>1.5/1.0$; a round edged cube was obtained as $R\langle 111\rangle/R\langle 110\rangle/R\langle 100\rangle \approx$ 1.4–1.6/1.2–1.3/1.0 and a spherical particle was obtained as $R\langle 111\rangle/R\langle 110\rangle/R\langle 100\rangle \approx 1.0/1.0/1.0$, as shown in Fig. 4.

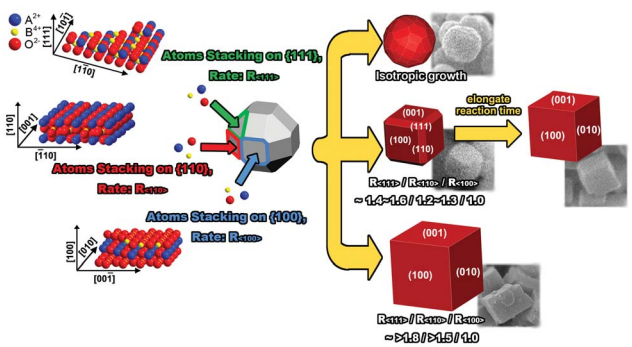

Fig. 4 The scheme of cubic crystal growth *via* different stacking rates (R) between the (100), (110) and (111) planes.

As we know, in Group 2 titanate perovskite ($A^{2+}B^{4+}O_3$), surfaces {100} consist of alternating neutral planes of AO and BO_2, making them nonpolar and stable.[15,16] On the other hand, the {111} surfaces of ABO_3, composed of alternating charged planes of AO_3 and B, are polar and reactive. In general, the charge density of alkali earth metal ions decreases in the order $Ca^{2+} > Sr^{2+} > Ba^{2+}$. Larger charge density of A^{2+} would make the layers more polar resulting in higher reactivity, which leads to fast stacking in this direction. Therefore the stacking rate on the {111} surfaces is CTO > STO > BTO. According to this analysis, CTO grows fast to get the large sized powder consisting of sharp-edged cubes while STO and BTO powders were made up of small sized cubes with rounded edges and spherical particles respectively.

Furthermore, the shape of STO can be manipulated by the reaction time. Round-edged STO cubes were obtained in a 48 hour experiment. In an attempt to synthesize STO cubes with sharp edges, the alkali treatment duration was increased. SEM and TEM images of the powders obtained from the reaction of TiO_2 with $Sr(OH)_2$ for 56 hours are shown in Fig. 5. The uniform cubic particles with sharp edges are about 100–180 nm in size, as shown in Fig. 5(a).

The TEM image of a sliced individual particle demonstrates the facet of the sharp-edged cube (Fig. 5(b)). The selected area electron diffraction pattern in Fig. 5(c) was analyzed along the diagonal of a cube which is shown in Fig. 5(b). The pattern demonstrates that the diffraction points were contributed by the {110} planes of single-crystalline STO along the [111] zone axis. According to stereographic projection along [111], the facets of the cube were assigned to the {100} planes. These observations indicate that there are two stages in the STO growth. In the early stage (before 48 h), the stacking rate ratios in {111}/{110}/{100} planes are about 1.4–1.6/1.2–1.3/1.0, resulting in the round-edged STO cubes. As crystals grow up (after 48 h), the surface area increases, resulting in larger exposure of unstable {111} planes, which leads to the growth in the ⟨111⟩ direction increase to minimize the surface energy; the sharp-edged cubes were obtained. It can be seen that the initial stage is anisotropic growth dominated and the following stage is surface energy controlled.

Conclusions

In this work, pure phase and well-crystallized ABO_3 materials, CTO, STO, BTO, and BST with different Ba contents were

 This journal is © The Royal Society of Chemistry 2012

View Article Online

Published on 30 January 2012. Downloaded by National Chiao Tung University on 28/04/2014 23:26:24.

successfully synthesized by alkali treatment using the corresponding Group 2 hydroxide at low temperature. In addition, the obtained powders in a 48 hour experiment are round, round-edged cubes and cubes with sharp edges for BTO, STO and CTO respectively. Furthermore, the morphologies of such perovskite materials could be tailored by altering the reaction time to obtain round, then round-edged cubic and then sharp-edged cubic particles. This phenomenon is due to the stability of different planes. Initially, all planes are exposed to particles, but as time progresses the least stable planes are the first to be hidden as they attract stacking atoms. For a short reaction time, all planes are exposed and round particles were obtained. When the reaction time was extended, less stable planes are hidden (round-edged cubes) until only the most stable faces, the {100} planes, are exposed (sharp-edged cubes). With morphological and compositional controllability, these materials may have specific applications in electro-optical and photocatalysts.[18–20]

Acknowledgements

The authors would like to thank the National Science Council of the Republic of China, Taiwan, for financially supporting this research under contract no. NSC 100-2113-M-007-006.

References

1 P. K. Galagher and J. Thompson, Jr, *J. Am. Ceram. Soc.*, 1965, **48**, 644; A. Beauger, J. C. Mutin and J. C. Niepce, *J. Mater. Sci.*, 1984, **19**, 195.
2 J. A. Rebane, Y. O. Gorbenko, S. G. Suslov, N. V. Yakovlev, I. E. Korsakov, V. A. Amelichev and Y. D. Tretyakov, *Thin Solid Films*, 1997, **302**, 140.
3 G. J. Choi, S. K. Lee, K. Woo, K. K. Koo and Y. S. Cho, *Chem. Mater.*, 1998, **10**, 4104.
4 M.-C. Tsai, J.-C. Chang, H,-S. Sheu, H.-T. Chiu and C.-Y. Lee, *Chem. Mater.*, 2009, **21**, 499.
5 S. O'Brien, L. Brus and C. B. Murray, *J. Am. Chem. Soc.*, 2001, **123**, 12085.
6 H. Shiibashi, H. Matsuda and M. Kuwabara, *J. Sol-Gel Sci. Technol.*, 1999, **16**, 129.
7 R. L. Brutchey and D. E. Morse, *Angew. Chem., Int. Ed.*, 2006, **45**, 6564.
8 R. K. Roeder and E. B. Slamovich, *J. Am. Ceram. Soc.*, 1999, **82**, 1665.
9 I. Sunagawa, *Crystals/Growth, Morphology, and Perfection*, Cambridge University Press, 2005, p. 60.
10 R. E. Reed-Hill and R. Abbaschian, *Physical Metallurgy Principles*, PWS Publishing, 3rd edn, 1994, p. 439.
11 L.-W. Yin, Y. Bando, J.-H. Zhan, M.-S. Li and D. Golberg, *Adv. Mater.*, 2005, **17**, 1972.
12 J. Chen, B. Wiley, Z.-Y. Li, D. Campbell, F. Saeki, H. Cang, L. Au, J. Lee, X. D. Li and Y. Xia, Gold nanocages, *Adv. Mater.*, 2005, **17**, 2255.
13 M. S. Hegde, K. Nagaveni and S. Roy, *Pramana J. Phys.*, 2005, **65**, 641.
14 V. F. Puntes, K. M. Krishnan and A. P. Alivisatos, *Science*, 2001, **291**, 2115.
15 J. Padilla and D. Vanderbilt, *Phys. Rev. B: Condens. Matter Mater. Phys.*, 1997, **56**, 1625.
16 V. E. Henrich and P. A. Cox, *The Surface Science of Metal Oxides*, Cambridge University Press, 1994, p. 38.
17 W. Kaminsky, *J. Appl. Crystallogr.*, 2005, **38**, 566; W. Kaminsky, *J. Appl. Crystallogr.*, 2007, **40**, 382.
18 D. Hennings, M. Klee and R. Waser, *Adv. Mater.*, 1991, **3**, 334.
19 T. Ohno, T. Tsubota, Y. Nakamura and K. Sayama, *Appl. Catal., A*, 2005, **288**, 74.
20 Y. Hu, O. K. Tan, J. S. Pan and X. Yao, *J. Phys. Chem. B*, 2004, **108**, 11214.
21 Y. J. Huang, H. T. Chiu and C. Y. Lee, *CrystEngComm*, 2009, **11**, 1904.